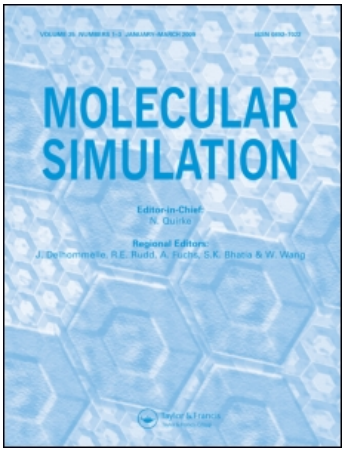

Molecular Simulation
Publication details, including instructions for authors and subscription information:
http://www.informaworld.com/smpp/title~content=t713644482

Isothermal-isobaric first-principles molecular-dynamics: application to polymorphism in liquids and amorphous materials

T. Morishita[a]
[a] Research Institute for Computational Sciences (RICS), National Institute of Advanced Industrial Science and Technology (AIST), Tsukuba, Ibaraki, Japan

To cite this Article Morishita, T.(2007) 'Isothermal-isobaric first-principles molecular-dynamics: application to polymorphism in liquids and amorphous materials', Molecular Simulation, 33: 1, 5 — 12
To link to this Article: DOI: 10.1080/08927020601071757
URL: http://dx.doi.org/10.1080/08927020601071757

Molecular Simulation, Vol. 33, Nos. 1–2, 15 January–15 February 2007, 5–12

Taylor & Francis
Taylor & Francis Group

Isothermal–isobaric first-principles molecular-dynamics: application to polymorphism in liquids and amorphous materials

T. MORISHITA*

Research Institute for Computational Sciences (RICS), National Institute of Advanced Industrial Science and Technology (AIST), 1-1-1 Umezono, Tsukuba, Ibaraki, 305-8568, Japan

(Received July 2006; in final form October 2006)

The capability of isothermal–isobaric first-principles molecular-dynamics (*NPT* FPMD) based on the combination of the Car–Parrinello, Andersen, and Nosé–Hoover techniques is illustrated by applications to polymorphism in liquids and amorphous materials. Recently, the possible existence of polyamorphic transitions has been extensively investigated in a variety of materials. Here we show *NPT* FPMD simulations of amorphous–amorphous transitions in silicon and liquid–liquid transitions in phosphorus. Both of these simulations are in excellent agreement with the recent experimental findings. The underlying mechanisms of these polyamorphic transitions have been clarified at an atomistic level.

Keywords: Polyamorphism; Extended Hamiltonian; First-principles; Molecular dynamics; Silicon; Phosphorus

1. Introduction

Molecular dynamics (MD) is a powerful tool for investigating a variety of phenomena in many-body systems. In particular, properties of condensed phases, such as liquids and solids, have been extensively investigated at an atomistic level. MD simulations are based on classical mechanics. The time evolution of each particle (atom or molecule) is usually determined by standard Newtonian or Hamiltonian dynamics. This means that, in standard MD simulations on condensed phases, the internal energy E as well as the number of particles N and the volume V is conserved: the microcanonical ensemble is generated. However, the conservation of E and V sometimes makes it difficult to directly compare MD results with experimental data. This is because temperature T and pressure P are kept constant instead of E and V in laboratory experiment. Also, it is not easy to simulate phenomena accompanying T and/or P changes which are often observed in experiment.

In order to overcome this difficulty, many extensions of MD calculation have been introduced. In 1980, Andersen introduced a pioneering technique [1] that enables the volume of a MD cell to vary while the pressure is maintained at a desired value. In this constant-pressure MD technique, the volume is regarded as one of dynamical variables and its value is determined by the balance between the internal pressure and the external pressure. This technique was further extended by Parrinello and Rahman [2] to deal with polymorphic transitions by allowing the shape of a MD cell as well as the volume to vary. The variable volume (and shape) especially aids in simulating phenomena accompanying large volume changes, e.g., phase transition.

Controlling temperature is also desirable because T is an experimentally controllable parameter. On the basis of Andersen's idea, Nosé proposed a Hamiltonian that produces MD trajectories following the canonical distribution [3,4]. He proved that averages over the MD trajectories from his Hamiltonian are equivalent to averages over the canonical ensemble. The temperature (i.e. an average of kinetic energy) is maintained at a desired value in Nosé's technique. We thus can easily deal with systems under desired temperature conditions. Hoover reformulated the equations from Nosé Hamiltonian and the resultant equations, Nosé–Hoover thermostat [5], have now widely been used. Both Andersen and Nosé's techniques are based on "extended" Hamiltonians

*Corresponding author. Email: t-morishita@aist.go.jp

Molecular Simulation
ISSN 0892-7022 print/ISSN 1029-0435 online © 2007 Taylor & Francis
http://www.tandf.co.uk/journals
DOI: 10.1080/08927020601071757

(Lagrangians) in which dynamical variables other than particles' positions and momenta are newly introduced. Combination of these two techniques is straightforward and the *NPT* ensemble, where *N*, *P*, and *T* are fixed as thermodynamic variables, can be generated from the Nosé–Andersen Hamiltonian [3,4].

The idea of the extended Hamiltonian formulation enables us not only to produce thermodynamic ensembles other than the microcanonical ensemble, but also to perform MD calculations with quantum mechanical description of interatomic forces, viz. first-principles molecular-dynamics (FPMD). Car and Parrinello introduced a new technique that unifies MD and electronic state calculations in the framework of classical machanics [6]. They postulated a Lagrangian in which the electronic wave functions ψ_i are regarded as dynamical variables. FPMD simulations can be performed by solving the equations of motion from the Car–Parrinello (CP) Lagrangian under the condition that electrons follow adiabatically the ionic motion remaining close to the Born–Oppenheimer (BO) surface. In the CP technique, the electronic states are calculated within density functional theory and interatomic forces are given by the Hellmann–Feynman theorem in the BO adiabatic approximation. It should be stressed here that the CP technique considerably reduces the computational cost for FPMD. This is reflected in the fact that the number of studies by FPMD has significantly increased since the Car–Parrinello technique was introduced.

We now easily recognize that isothermal–isobaric FPMD (*NPT* FPMD) can be performed by combining above three extended MD techniques. *NPT* FPMD is particularly of use to investigate phase transitions because interatomic interactions, i.e. electronic states, change significantly in phase transitions that are typically induced by *T* or *P* changes accompanying the volume changes. In fact, polymorphic transitions in various materials have extensively been studied by using *NPT* FPMD [7,8,9,10].

Recently, polymorphism in liquids and glasses, *polyamorphism*, has attracted significant attention because of its potential for new properties or functions [11]. In 1984, a distinct second amorphous form of water, high-density amorphous (HDA) water, was discovered by pressurizing crystalline ice (Ih) at very low temperature [12]. This experimental observation has triggered subsequent extensive investigations on polyamorphism in water and other substances [13]. In particular, much work has focused on substances with directional bonding, such as water, silica, Si, and phosphorus (P) [11–20]. It is well recognized that microscopic approaches are crucial in clarifying underlying mechanisms of polyamorphism. We thus consider that *NPT* FPMD simulations should be of great use to explore polyamorphs of a variety of substances.

In this paper, we demonstrate *NPT* FPMD simulations of polyamorphic transitions in amorphous Si and liquid P. In the next section, *NPT* FPMD method is briefly reviewed. The simulations of polyamorphic transitions in amorphous Si and liquid P are presented in Section 3 and 4, respectively, and conclusions are drawn in Section 5.

2. Isothermal–isobaric Car–Parrinello molecular dynamics

The combination of the three extended MD techniques is the key in order to perform *NPT* FPMD simulations. We first construct the CP Lagrangian incorporating the Andersen's constant-pressure technique, and then we introduce Nosé–Hoover thermostats, one for the ionic and one for the electronic systems, to ensure the adiabatic separation between these systems. It should be noted that it is difficult to construct the Lagrangian (or Hamiltonian) incorporataing these three extended techniques, because we cannot attach the same thermostat to both the ionic and electronic systems; the adiabatic separation should be preserved during MD runs.

In the Andersen's constant-pressure technique, the volume of a MD cell, *V*, is regarded as a dynamical variable and the coordinates and velocities of the ions are expressed in the following scaled forms: [1,2],

$$\mathbf{R}_I = V^{1/3}\mathbf{s}_I, \tag{1}$$

$$\mathbf{v}_I = V^{1/3}\dot{\mathbf{s}}_I, \tag{2}$$

where $\mathbf{R}_I$ is the real coordinate, $\mathbf{s}_I$ is the scaled coordinate ($0 \le s_{Ix}, s_{Iy}, s_{Iz} \le 1$), and $\mathbf{v}_I$ is the real velocity of ion *I*. We here assume a cubic MD cell with a side $V^{1/3}$ long. The single electron orbitals ψ_i are also expressed in a similar scaling relation [7],

$$\psi_i(\mathbf{r}) = \frac{1}{\sqrt{V}}\varphi_i(V^{1/3}\mathbf{s}). \tag{3}$$

By use of these relations, the Lagrangian of the constant-pressure CP dynamics is given as

$$\begin{aligned} L = &\sum_i \mu \int |\dot{\varphi}_i|^2 \mathrm{d}\mathbf{s} + \frac{1}{2}\sum_I M_I V^{2/3}\dot{\mathbf{s}}_I^2 \\ &- E[\{\varphi_i\}, \{V^{1/3}\mathbf{s}_I\}] + \frac{1}{2}W\dot{V} - P_{\mathrm{ex}}V \\ &+ \sum_i\sum_j \varepsilon_{ij}\left(\int \varphi_i^*\varphi_j \,\mathrm{d}\mathbf{s} - \delta_{ij})\right). \end{aligned} \tag{4}$$

The first term is a fictitious kinetic energy of the φ_i and μ is a mass parameter associated with the φ_i. The second term is an ionic kinetic energy and the fourth term is that of *V*, where *W* is a mass parameter associated with *V*. *E* is the potential energy surface depending on both the $\mathbf{R}_I$ and $\psi_i(\mathbf{r})$, and P_{ex} is the external pressure. The Lagrangian multipliers ε_{ij} are introduced to impose the orthonormality constraints on the φ_i. The equations of motion for φ_i, $\mathbf{s}_I$,

and V are thus derived as

$$\mu\ddot{\varphi}_i(\mathbf{r}) = -\frac{\delta E}{\delta\varphi_i^*(\mathbf{r})} + \sum_j \varepsilon_{ij}\varphi_j(\mathbf{r}), \tag{5}$$

$$M_I\ddot{\mathbf{s}}_I = -V^{-2/3}\frac{\partial E}{\partial \mathbf{s}_I} - M_I\frac{2\dot{V}}{3V}\dot{\mathbf{s}}_I, \tag{6}$$

$$W\ddot{V} = \left[\frac{1}{3V}\sum_I M_I V^{2/3}\dot{\mathbf{s}}_I^2 - \frac{\partial E}{\partial V}\right] - P_{\mathrm{ex}}. \tag{7}$$

Integrating these equations, FPMD under a constant-pressure condition can be implemented as far as the φ_i are maintained close to the BO trajectory.

In order to produce constant temperature conditions and to ensure the adiabatic separation between the ionic and electronic systems, two Nosé–Hoover thermostats are introduced; one for the ionic and one for the electronic degrees of freedom [21]. The time evolution of the thermostat variables, ζ and ξ for the ionic and electronic systems, respectively, is determined by the following equations,

$$Q_{\mathrm{ion}}\dot{\zeta} = \left(\sum_I M_I V^{2/3}\dot{\mathbf{s}}_I^2 - N_{\mathrm{ion}}k_B T_{\mathrm{ion}}\right), \tag{8}$$

$$Q_{\mathrm{wf}}\dot{\xi} = \left(\sum_i 2\mu\int|\dot{\varphi}_i|^2 \mathrm{d}\mathbf{s} - N_{\mathrm{wf}}k_B T_{\mathrm{wf}}\right), \tag{9}$$

where N_{ion} and N_{wf} are the number of degrees of freedom in the ionic and electronic systems, respectively, and T_{ion} and T_{wf} are the temperature of the ionic and electronic systems, respectively. Q_{ion} and Q_{wf} are mass parameters for ζ and ξ, and k_B is Boltzmann's constant. We remark that T_{wf} is much lower than T_{ion} because the φ_i should be very close to the BO surface during MD runs [21]. Also note that the periodic resetting of the total ionic momentum is necessary in metallic systems to suppress the ionic flow due to the thermostats [22].

FPMD under a constant-pressure condition takes more computational cost than the standard FPMD. In the plane-wave basis representaion, the matrix elements are functions of reciprocal vectors and are usually calculated only once in a preparation process before MD runs in standard constant-volume FPMD. However, in the case that the volume (and shape) of a MD cell can vary during MD runs, reciprocal vectors and thus the matrix elements are recalculated at every time step. This considerably raises the computational cost in constant-pressure FPMD. Consequently, *NPT* FPMD has been limited to relatively small systems and short simulation time to this time. Owing to this short simulation time, we often have to over-pressurize our systems to induce structural transformations during the limited simulation time. Periodic boundary conditions and a systematic underestimation of the internal pressure may also be responsible for the over-pressurization (the latter is especially crucial in FPMD calculations [20]). Extreme care therefore should be taken in *NPT* FPMD simulations of phase transitions (see [16] for amorphous Si and [23,20] for liquid P).

In our calculations, cubic MD cells containing 64 atoms were employed with periodic boundary conditions. The electronic wave functions for occupied valence states were expanded in a plane wave basis with an energy cutoff of 20Ry for Si and of 30Ry for P at the Γ point in the Brillouin zone. The same basis set was used during a MD run even when drastic volume changes occurred. The electron-ion interaction was described by a norm-conserving pseudpotential [24] with a separable form [25]. The exchange-correlation energy was treated in the local density approximation and a parameterized form by Perdew and Zunger [26] was used. The equations of motion for *NPT* FPMD were integrated with a time step of 0.121 fs, and the mass parameters were set as follows: $\mu = 500$ a.u., $Q_{\mathrm{ion}} = 250{,}000$ a.u., and $Q_{\mathrm{wf}} = 1400$ a.u.

3. Polyamorphism in amorphous Si

3.1 Background

Silicon has several characteristics that are also exhibited in water: (1) locally tetrahedral coordination; (2) denser liquid than its crystalline form; and (3) a negative slope in the T–P melting curve. It is considered that these characteristics may play a crucial role in polyamorphism in Si and water [11]. However, much less has been understood about polyamorphism in Si than in water. In this section, *NPT* FPMD simulations of polyamorphic transformations of amorphous Si are demonstarated. In our calculations, we have found out a new HDA form of Si by pressurizing a low-density amorphous (LDA) form (normal amorphous Si with tetrahedral coordination). The new amorphous form has higher density than LDA, and is completely different from the HDA form observed in the recent *ab initio* calculations [15] (we refer to this previously reported form as very high-density amorphous (VHDA) form). Detailed structural analysis has shown that the new HDA form has coordination ~ 5 and has analogous structure of HDA water (ice) [16].

3.2 Results

A new HDA form of Si was obtained by pressurizing a LDA form (normal amorphous Si) at ~ 300 K. LDA Si was prepared by rapid quenching of a liquid Si (*l*-Si) at atmospheric pressure; the structure of the LDA form thus obtained agrees well with the previously reported amorphous structure [27] that has locally tetrahedral coordination. In pressurization, LDA was preserved until the external pressure reached 12 GPa. However the volume suddenly decreased at 12 GPa as shown in figure 1, indicating transformation to a HDA form. Figure 2 shows the pair correlation functions $g(r)$ for the LDA and the resulting HDA forms. It is striking that the transformed amorphous form has completely different characteristics

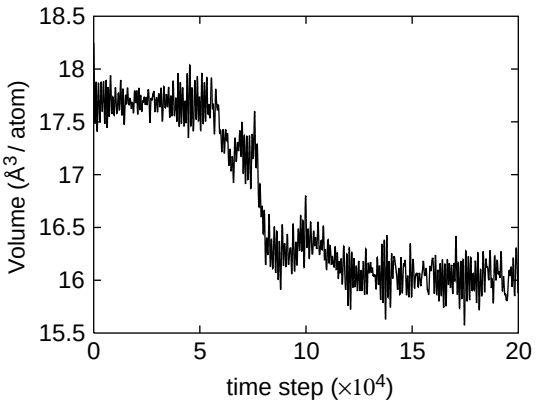

Figure 1. Time evolution of the volume per atom in the LDA to HDA transition in Si.

from those of LDA. Remarkable changes are found in the first peak and the first minimum. The broadening of the first peak indicates degradation of covalent bonds that form locally tetrahedral configurations at low pressures. The change around the first minimum affects the coordination number N_c that is obtained by integrating $4\pi r^2\rho^* g(r)$ up to the first minimum r_m, where ρ^* is the number density. N_c of LDA is 4.0 reflecting tetrahedral coordination, whereas that of HDA is calculated as 5.1. To get a deeper insight into the structural differences, the bond-angle distribution function $A(\theta)$ is calculated for LDA and HDA (figure 3). $A(\theta)$ counts angles between the two vectors that join a central atom with two neighbors within a sphere of radius r_m. LDA has a single peak around 109.5° reflecting the tetrahedral configuration. In contrast, the main peak in HDA is broadened and the peak position is shifted to ∼90°. Detailed analysis shows that the first four neighbors in HDA still form a (slightly deformed) tetrahedral structure, but the fifth neighbor is located at an open space of the tetrahedron. It can be considered that the HDA structure is formed by forcing the fifth neighboring atom, which is outside the first coordination shell in LDA, into the interstitial position. This structure is completely different from that of the VHDA form [15]. N_c of VHDA is 8–9, and a distinct peak at ∼60° is found in $A(\theta)$ for

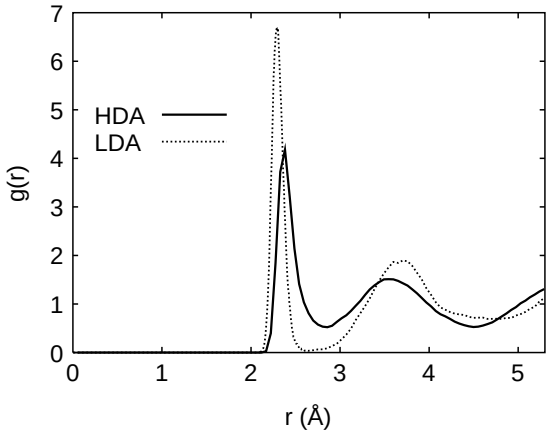

Figure 2. Pair correlation functions $g(r)$ for HDA (solid lines) and LDA (dashed lines).

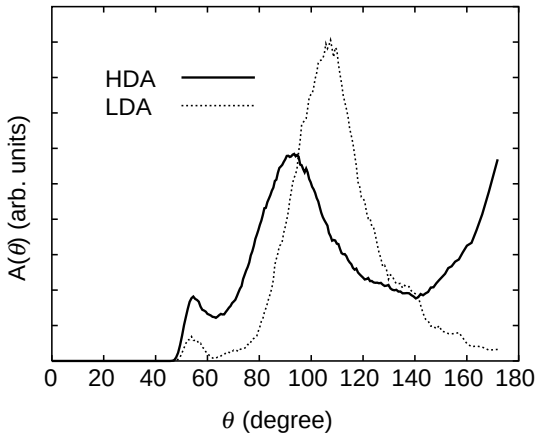

Figure 3. Bond-angle distribution functions $A(\theta)$ for HDA (solid lines) and LDA (dashed lines).

VHDA [15], indicating more close-packed structure than HDA. Interestingly, N_c of LDA, HDA and VHDA roughly coincide with those of the crystalline forms of Si, viz. the diamond, β-tin and sh structures, respectively (note that the latter two are high-pressure forms and N_c of diamond, β-tin and sh is 4, 6 and 8, respectively [28]). Both the HDA and the β-tin structure contain deformed tetrahedra with interstitial atoms resulting in N_c of 5–6. The reported VHDA form partially contains sh-like configurations and N_c is between 8 and 9 [15]. It is therefore likely that the trend in crystalline forms is preserved in amorphous forms, and that HDA is located between LDA and VHDA in the phase diagram. The VHDA form may result from an incomplete crystallization of the sh structure. It is worth noting that the third distinct amorphous form with coordination ∼9 has also been observed in water (VHDA ice) [29].

Figure 4 shows typical Atomic configurations of LDA and HDA Si. The HDA structure of Si is almost the same as that of water (ice). Each water molecule in HDA ice is tetrahedrally coordinated as in LDA ice, but an interstitial molecule is present in the first coordination shell [30]. It is thus considered that the LDA-HDA transformation of Si in the present simulation has a strong resemblance to that of ice.

We have also found that LDA can be recovered by depressurization as in amorphous ice. Upon release of the pressure at 300 K, HDA was still preserved at 0 GPa, but heating induced transformation to LDA. The reverse transformation was initiated at ∼700 K. $g(r)$ for the amorphous form thus obtained has a sharp first peak containing four nearest neighbors and distinct separation between the first and second peaks. It is clearly shown that HDA was reversely transformed to LDA. The reversible LDA-HDA transition in the present calculations is in excellent agreement with recent experimental observations [17].

Our analyses have clarified that structures of HDA and quenched *l*-Si under pressure are based on the same framework; distorted tetrahedra with interstitial atoms. In fact, the HDA form can be obtained not only by pressuring a LDA form but also by vitrifying a *l*-Si under pressure in

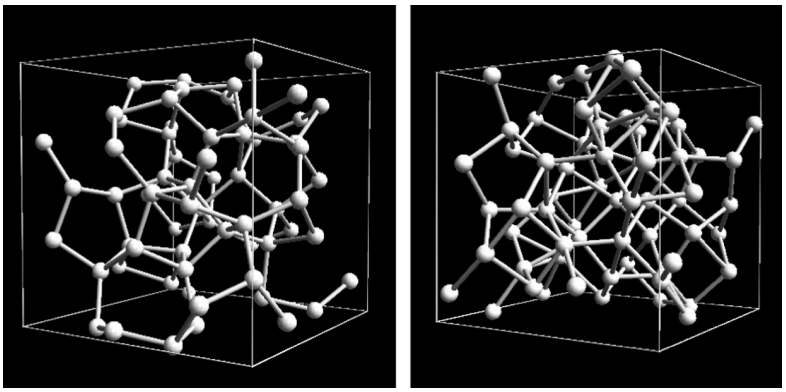

Figure 4. Atomic configurations of LDA (left) and HDA (right).

our simulations [16]. Considering the structural similarity and the vitrification under pressure, we reach the conclusion that supercooled *l*-Si under pressure is directly connected with HDA. It appears that the reduction of the tetrahedral configuration followed by interstitial atoms plays a key role in disordered phases of Si under pressure. The stability of the tetrahedral configuration may be used as a kind of order parameter to classify disordered states of Si.

3.3 Summary of amorphous–amorphous transition of Si

We have found out a new HDA form of Si with coordination ~ 5 in isothermal–isobaric FPMD simlations. The structure of the new HDA Si is very close to that of HDA ice, but is completely different from that of VHDA Si. It is found that HDA is reversely transformed to LDA by depressurization and heating. Remarkable similarities between HDA Si and HDA ice would improve our understanding of the phase diagram of disordered phases. Also, this similarity leads to the conjecture that HDA ice is continuously connected with supercooled liquid water under pressure. Finney *et al.* have pointed out the similarities of local structures between HDA ice and supercooled liquid water under pressure [30]. Although glassy pure water under pressure has not been directly obtained in experiment, a recent MD study reports a consistent result with this conjecture [31]. We expect that the present findings will stimulate further investigations on polyamorphism in Si, water, and other substances with tetrahedral coordination such as germanium and carbon.

4. Polyamorphism in liquid phosphorus

4.1 Background

Recently, a first-order transition between two distinct liquid phases, liquid–liquid transition, has been experimentally observed in phosphorus [18]. Under low pressure (<1 GPa), liquid P (*l*-P) can be obtained by melting black P (A17 crystal) that is the most stable allotrope of P under ambient conditions. This low-density liquid (LDL) consists of tetrahedral P_4 molecules (a molecular liquid) and is considered to be identical to a liquid obtained by melting white P. Katayama and coworkers observed drastic changes of structure factor $S(Q)$ and the density of *l*-P by pressure changes around 1 GPa and 1400 K [18]. The measured $S(Q)$ for a high-density liquid (HDL) transformed from LDL is consistent with the form having a polymeric network in which atoms are connected by anisotropic bonds without forming any molecules [18].

In order to clarify the mechanism of the liquid–liquid transition and liquid structure of HDL P at an atomistic level, we carried out *NPT* FPMD simulations of the liquid–liquid transition of P [19]. The process of the polymerization of the P_4 molecules by heating was previously investigated by FPMD calculations by Hohl and Jones [32]. They however, performed constant-volume calculations, so that the density changes, which are crucial in liquid–liquid transition, were not reproduced. In our calculations, the constant-pressure condition enables us to reproduce the drastic density changes in liquid–liquid transitions: the importance of the constant-pressure condition is clearly demonstrated.

4.2 Results

In the present calculations, a LDL form of P was prepared by heating the initial arrangement of 16 P_4 tetrahedra (64 P atoms) in the bcc structure. Over ~ 1000 K, P_4 tetrahedra began to diffuse, and the molecular liquid (LDL) was obtained after annealing for ~ 4 ps at 1400 K. In order to adjust the density to ~ 1.6 g/cm^3 at 1400 K [33], the external pressure was set to 0.7 GPa.

In a pressurization process, the external pressure was changed from 0.7 to 2.5 GPa in a stepwise manner maintaining the temperature at 1400 K. Figure 5 shows the time evolution of the volume per atom in the LDL–HDL transition. At time step 17,000, LDL is pressurized to 2.5 GPa and the volume instantaneously shrinks with $\sim 40\%$ reduction (density is increased to 2.77 g/cm^3 [33]). The pair correlation function $g(r)$ was calculated before

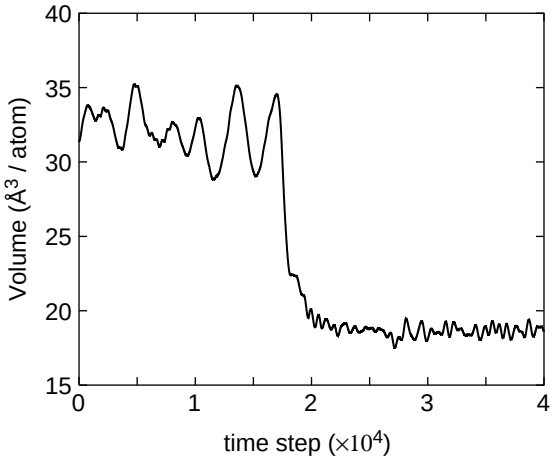

Figure 5. Time evolution of the volume per atom in the LDL to HDL transition in P. LDL is pressurized from 0.7 to 2.5 GPa at time step 17,000.

and after the pressurization. The upper panel in figure 6 shows $g(r)$ at 0.7 GPa (LDL) and lower panel shows $g(r)$ at 2.5 GPa (HDL). At 0.7 GPa, $g(r)$ exhibits characteristics of the tetrahedral molecular liquid. The first peak reflects the distribution of the interatomic distance within the tetrahedral P_4 molecules. The coordination number N_c obtained by integrating $4\pi r^2\rho^* g(r)$ up to the first minimum r_m (2.6 Å) is 3.0, which clearly reflects the existence of the tetrahedral molecule. The overall shape of $g(r)$ agrees well with the previous theoretical and experimental results of the molecular liquid [18,32].

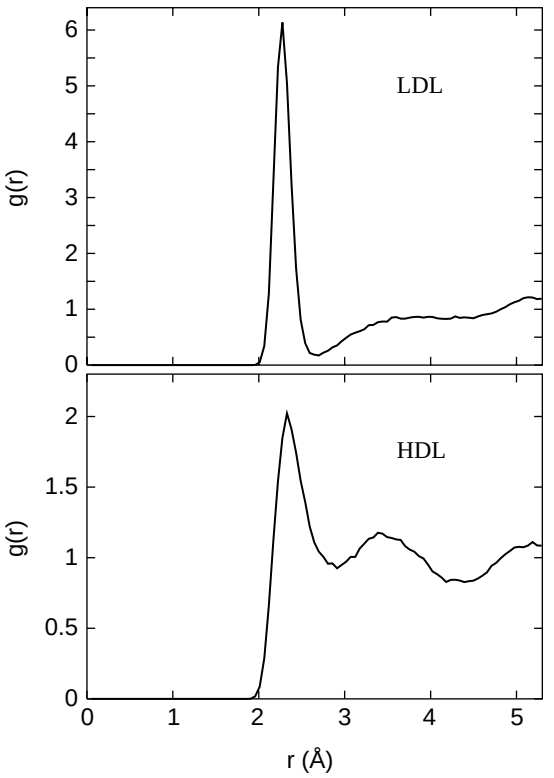

Figure 6. Pair correlation functions $g(r)$ for the molecular liquid (LDL) and polymeric liquid (HDL).

At 2.5 GPa, $g(r)$ shows completely different characteristics from those of LDL. The first peak becomes much broader and the second peak (around 3.5 Å) emerges which cannot be seen in $g(r)$ for LDL. These characteristics are similar to those of liquid arsenic (l-As) that has a polymeric form [34,35]. N_c for HDL is calculated as 4.1 by taking r_m as 2.8 Å. This value is slightly larger than that of l-As ($N_c \sim 3.6$) [34,35], but this is due to the higher pressure (2.5 GPa) in the present simulations. It has been found that N_c is ~ 3.7 at 1 GPa for this polymeric phase of l-P [23].

Figure 7 shows $S(Q)$ for LDL and HDL together with experimental results [18]. The calculated $S(Q)$ both for LDL and HDL are in good agreement with experimentally measured $S(Q)$. In particular, the shifts of the peak positions resulting from the LDL–HDL transition are well reproduced in our calculations. The two characteristic peaks (around 2.5 and 3.7 $Å^{-1}$) of $S(Q)$ for HDL indicate a more complicated liquid structure than that of a simple liquid. These two peaks are more clearly reproduced than the previous FPMD result of l-As [34] but not completely yet. This might be due to the small system size in our calculations.

A snapshot of a typical atomic configuration of HDL is given in figure 8. It is apparent that all tetrahedral molecules collapse and a polymeric network form is

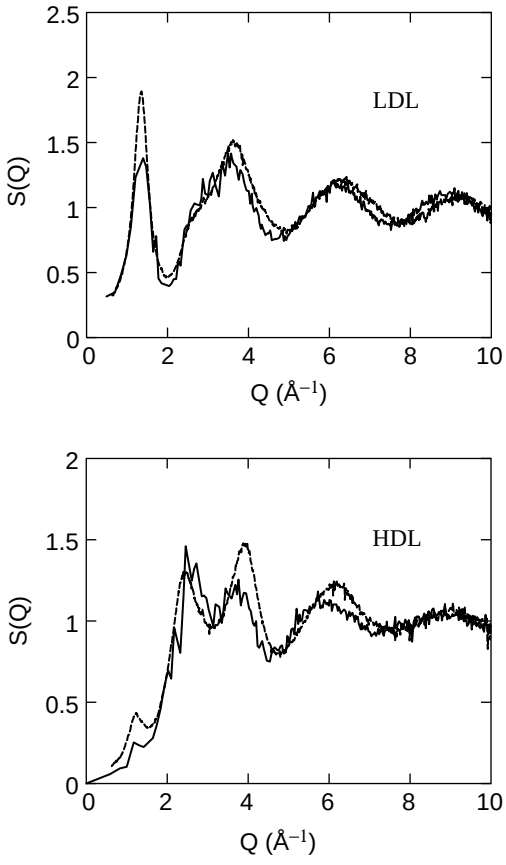

Figure 7. Structure factors $S(Q)$ for the molecular liquid (LDL) and polymeric liquid (HDL). The simulation results (solid lines) are compared with the experimental results (dashed lines) [18].

generated after the LDL-HDL transition. The formation of a dense network configuration is consistent with the result by Hohl and Jones [32].

The electronic densities of states (DOS) for LDL and HDL are shown in figure 9. In the molecular phase, we see three separated bands below the Fermi energy E_F with a gap at the E_F. These characteristic bands are also seen in the DOS for an isolated P_4 molecule, which indicates the weak interactions between the molecules. The DOS for the polymeric phase does not have a gap around the E_F showing a metallic-like character. Valence bands are split around -6 eV: the lower and upper parts mainly consist of *s* and *p* bands, respectively. That is, atomic bonds are mainly composed of the *p*-state electrons. It is also found that the *p* band has a dip at the E_F. This indicates that the Peierls-like distortion exists in HDL P as in the A7 crystalline P. It has been shown that the Peierls distortion is caused only by atomic interactions within a certain local region around each atom, not by periodicity [36]. Details of the Peierls-like distortion in *l*-P are discussed in Ref. [23]

4.3 Summary of liquid–liquid transition of P

Liquid–liquid phase transition of phosphorus was successfully simulated in isothermal–isobaric FPMD calculations. The present calculations show that the transition is caused by the breakup of P_4 tetrahedral molecules and that the polymeric liquid (HDL) is generated accompanying significant volume contraction. Owing to the constant-pressure condition, the volume change was clearly reproduced. Our simulations have revealed that the collapse of the open atomic configuration plays an important role in the liquid–liquid transition of phosphorus.

We also found that electronic states drastically change in the transition. It is shown that atomic bonds are mainly composed of the *p*-state electrons in HDL as in the crystalline phases of P. There exists a dip at the E_F in the DOS for HDL and the dip separates the bonding and anti-bonding *p*-states. This indicates that the Peierls-like distortion, which is observed in the crystalline structure (A7), is still preserved in the polymeric phase of *l*-P.

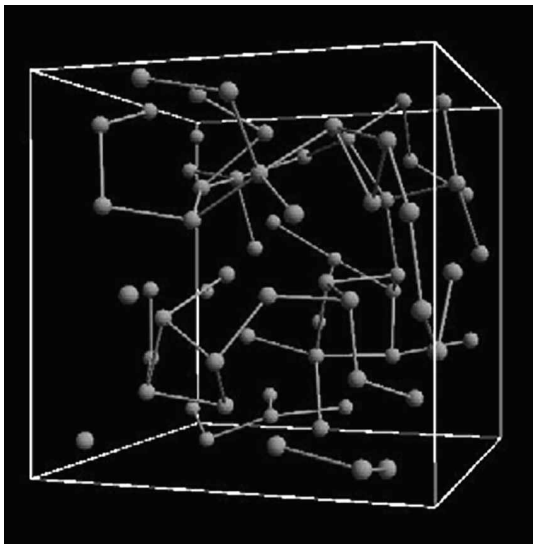

Figure 8. Snapshot of an atomic configuration in HDL P.

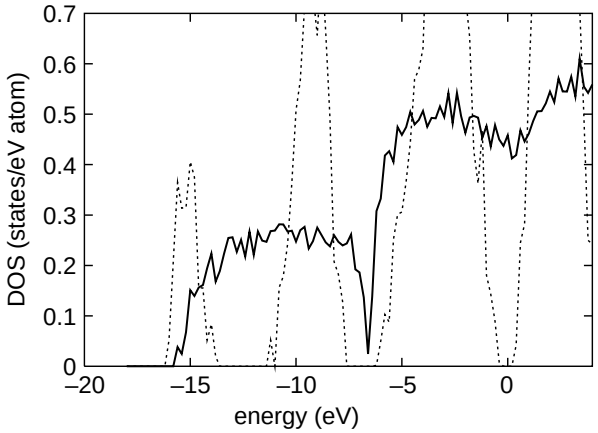

Figure 9. The electronic densities of state (DOS) for HDL (solid lines) and LDL (dashed lines).

5. Conclusions

We have demonstrated the capability of *NPT* FPMD for investigating polymorphism in liquids and amorphous materials. Our calculations have revealed drastic structural changes induced by *P* and/or *T* changes in amorphous Si and liquid P, which are consistent with the recent experimental findings. In liquid and glassy phases, there exists a variety of interatomic interactions, in contrast to crystalline phases, reflecting disorderd atomic configurations. This prevents us from constructing interatomic potentials that well reproduce physical properties of liquids and glasses under various pressure and temperature conditions. *NPT* FPMD is thus suitable to investigate such disordered systems in a wide pressure and temperature range. Recently, polyamorphic transitions have been observed not only in single component systems but also in much more complicated systems such as Y_2O_3–Al_2O_3 and triphenyl-phosphite [37,38]. Although it is not easy to perform FPMD on such systems because of its high computational cost at present, we believe that recent progress in algorithms and high performance computers enables us to investigate such complicated systems by *NPT* FPMD in the near future.

Acknowledgements

I wish to thank the late professor Shuichi Nosé for helpful comments and continual encouragement. I also thank him for his guidance during my PhD period. I wish to pray for the repose of his soul. The computations were carried out

at the Research Center for Computational Science, National Institute of Natural Sciences.

References

[1] H.C. Andersen. Molecular dynamics simulations at constant pressure and/or temperature. *J. Chem. Phys.*, **72**, 2384 (1980).

[2] M. Parrinello, A. Rahman. Crystal structure and pair potentials: a molecular-dynamics study. *Phys. Rev. Lett.*, **45**, 1196 (1980).

[3] S. Nosé. A molecular dynamics method for simulations in the canonical ensemble. *Mol. Phys.*, **52**, 255 (1984).

[4] S. Nosé. A unified formulation of the constant temperature molecular dynamics methods. *J. Chem. Phys.*, **81**, 511 (1984).

[5] W.G. Hoover. Canonical dynamics: equilibrium phase-space distributions. *Phys. Rev. A*, **31**, 1695 (1985).

[6] R. Car, M. Parrinello. Unified approach for molecular dynamics and density-functional theory. *Phys. Rev. Lett.*, **55**, 2471 (1985).

[7] P. Focher, G.L. Chiarotti, M. Bernasconi, E. Tosatti, M. Parrinello. Structural phase transformations via first-principles simulation. *Europhys. Lett.*, **26**, 345 (1994).

[8] S. Scandolo, M. Bernasconi, G.L. Chiarotti, P. Focher, E. Tosatti. Pressure-induced transformation path of graphite to diamond. *Phys. Rev. Lett.*, **74**, 4015 (1995).

[9] R.M. Wentzcovitch. hcp-to-bcc pressure-induced transition in Mg simulated by *ab initio* molecular dynamics. *Phys. Rev. B*, **50**, 10358 (1994).

[10] T. Morishita, S. Nosé. Examination of structural stability and phase transitions in constant-pressure first-principles molecular dynamics simulations. *Mol. Simul.*, **28**, 249 (2002).

[11] P.H. Poole, T. Grande, C.A. Angell, P.F. McMillan. Polymorphic phase transitions in liquids and glasses. *Science*, **275**, 322 (1997).

[12] O. Mishima, L.D. Calvert, E. Whalley. 'Melting ice' I at 77 K and 10 kbar: a new method of making amorphous solids. *Nature*, **310**, 393 (1984).

[13] O. Mishima, H.E. Stanley. The relationship between liquid, supercooled and glassy water. *Nature*, **396**, 329 (1998).

[14] D.J. Lacks. First-order amorphous–amorphous transformation in silica. *Phys. Rev. Lett.*, **84**, 4629 (2000).

[15] M. Durandurdu, D.A. Drabold. *Ab initio* simulation of first-order amorphous-to-amorphous phase transition of silicon. *Phys. Rev. B*, **64**, 014101 (2001).

[16] T. Morishita. High density amorphous form and polyamorphic transformation of silicon. *Phys. Rev. Lett.*, **93**, 055503 (2004).

[17] P.F. McMillan, M. Wilson, D. Daisenberger, D. Machon. A density-driven phase transition between semiconducting and metalllic polyamorphs of silicon. *Nat. Matter.*, **4**, 680 (2005).

[18] Y. Katayama, T. Mizutani, W. Utsumi, O. Shimomura, M. Yamakata, K. Funakoshi. A first-order liquid–liquid phase transition in phosphorus. *Nature*, **403**, 170 (2000).

[19] T. Morishita. Liquid–liquid phase transitions of phosphorus via constant-pressure first-principles molecular dynamics simulations. *Phys. Rev. Lett.*, **87**, 105701 (2001).

[20] L.M. Ghiringhelli, E.J. Meijer. Phosphorus: first principles simulation of a liquid–liquid phase transition. *J. Chem. Phys.*, **122**, 184510 (2005).

[21] P. Blöchl, M. Parrinello. Adiabaticity in first-principles molecular dynamics. *Phys. Rev. B*, **45**, 9413 (1992).

[22] T. Morishita, S. Nosé. Momentum conservation law in the Car–Parrinello method. *Phys. Rev. B*, **59**, 15126 (1999).

[23] T. Morishita. Polymeric liquid of phosphorus at high pressure: first-principles molecular-dynamics simulations. *Phys. Rev. B*, **66**, 054204 (2002).

[24] G.B. Bachelet, D.R. Hamann, M. Schlüter. Pseudopotentials that work: from H to Pu. *Phys. Rev. B*, **26**, 4199 (1982).

[25] L. Kleinman, D.M. Bylander. Efficacious form for model pseudopotentials. *Phys. Rev. Lett.*, **48**, 1425 (1982).

[26] J. Perdew, A. Zunger. Self-interaction correction to density-functional approximation for many electron systems. *Phys. Rev. B*, **23**, 5048 (1981).

[27] I. Štich, R. Car, M. Parrinello. Amorphous silicon studied by *ab initio* molecular dynamics: preparation, structure, and properties. *Phys. Rev. B*, **44**, 11092 (1991).

[28] A. Mujica, A. Rubio, A. Muñoz, R.J. Needs. High-pressure phases of group-IV, III–V, and II–VI compounds. *Rev. Mod. Phys.*, **75**, 863 (2003).

[29] T. Loerting, C. Salzmann, I. Kohl, E. Mayer, A. Hallbrucker. A second distinct structural "state" of high-density amorphous ice at 77 K and 1 bar. *Phys. Chem. Chem. Phys.*, **3**, 5355 (2001).

[30] J.L. Finney, A. Hallbrucker, I. Kohl, A.K. Soper, D.T. Bowron. Structures of high and low density amorphous ice by neutron diffraction. *Phys. Rev. Lett.*, **88**, 225503 (2002).

[31] B. Guillot, Y. Guissani. Polyamorphism in low temperature water: a simulation study. *J. Chem. Phys.*, **119**, 11740 (2003).

[32] D. Hohl, R.O. Jones. Polymerization in liquid phosphorus: simulation of a phase transition. *Phys. Rev. B*, **50**, 17047 (1994).

[33] Y. Katayama, Y. Inamura, T. Mizutani, M. Yamakata, W. Utsumi, O. Shimomura. Macroscopic separation of dense fluid phase and liquid phase of phosphorus. *Science*, **306**, 848 (2004).

[34] X.-P. Li. Properties of liquid arsenic: a theoretical study. *Phys. Rev. B*, **41**, 8392 (1990).

[35] C. Bichara, A. Pellegatti, J.-P. Gaspard. Properties of liquid group-V elements: a numerical tight-binding simulation. *Phys. Rev. B*, **47**, 5002 (1993).

[36] J.P. Gaspard, F. Marinelli, A. Pellegatti. Peierls instabilities in covalent structures. *Europhys. Lett.*, **3**, 1095 (1987).

[37] S. Aasland, P.F. McMillan. Density-driven liquid–liquid separation in the system Al_2O_3–Y_2O_3. *Nature*, **369**, 633 (1994).

[38] R. Kurita, H. Tanaka. Critical-like phenomena associated with liquid—liquid transition in a molecular liquid. *Science*, **306**, 845 (2004).